Structures 57 (2023) 105314

Contents lists available at ScienceDirect

Structures

journal homepage: www.elsevier.com/locate/structures

Damage detection, localization, and quantification for steel cables of post-tensioned bridge decks

Isabella Mazzatura [a,*], Walter Salvatore [a], Silvia Caprili [a], Simone Celati [a], Michele Mori [b], Massimo Gammino [b]

[a] *Department of Civil and Industrial Engineering, University of Pisa, Pisa, Italy*
[b] *SINA Site Service S.p.A (ASTM Group), Milano, Italy*

A R T I C L E I N F O

Keywords:
Post-tensioned concrete bridges
Assessment
Non-destructive testing methods
Ultrasonic tomography
GPR
X-ray diffraction

A B S T R A C T

The present work aims to provide an in-situ inspection methodology for prestressed concrete bridges with post-tensioned cables (PT bridges). The adoption of non-destructive techniques (NDT), already widely employed in other engineering fields, is proposed, providing reliable information with a relatively low impact on the existing infrastructure. For each of the specific inspection topics (i.e. cables' layout detection, defect localization and quantification, estimation of residual prestressing force) the proposed investigation procedure was calibrated through a deep experimental test campaign, including both laboratory tests – planned and performed to validate the method and check its efficiency and reliability – and applications to existing viaducts located on the Italian highways.

1. Introduction

Prestressed concrete bridges with post-tensioned (PT) tendons represent a relevant percentage of the current Italian infrastructural heritage. The rise of this constructive technology coincided with the economic boom: lots of bridges were built adopting such construction technique thanks to its advantages over traditional Reinforced Concrete (RC). The repeatability of the static scheme, the easy application to different sites, the quick construction process thanks to partial prefabrication, the ability to cover longer spans using fewer materials' amount than RC infrastructures and the higher quality resulting from a more strict and controlled construction process are only some of the benefits.

Recent catastrophic events, on the other hand, highlighted the need for the assessment of PT structures and the unreliability of using only visual inspections to analyze their maintenance condition since an (apparent) good state of conservation does not always determine a safe system. The main issue is the presence of hidden defects, not visible and not detectable through only visual surveys but responsible for most of the structural deficiencies in PT bridges. Among them, corrosion of steel PT cables with degradation of the mechanical properties [1] and of the overall structural performance represent one of the most critical situations. Defects in the grouting can promote degradation leading to unexpected failures even without relevant traffic loads acting on the deck [2]. Deterioration impacts internal tendons, modifying the stresses' distribution within the beam and promoting strands' corrosion, leading to the progressive loss of strands' strength and the global pre-stressing force in the concrete and the arising of cracks and permanent deformations [3–7]. Therefore, the residual performance of corroded strands depends on the typology, localization and entity of the defects, as well as the definition of the effective residual tension acting on PT tendons, influencing the global bridge performance. The lack (or segregation) of the mortar within the ducts [8,9] and the presence of water need therefore to be deeply investigated; recent research focused on methods to identify grouting defects and cables' corrosion.

In 2020 the Italian Ministry of Infrastructures and Transportation enacted specific guidelines for the risk classification, monitoring and assessment of existing bridges [10]. Progressive in-depth approaches were suggested, ranging from simple visual in-situ inspections for most infrastructures to specific survey procedures (the so-called Special Inspections - SI) for PT bridges. However, the methodology for SI is not clearly defined; suggestions on possible survey and testing techniques are given but specific indications are missing, and the unreliability/inefficiency of methodologies used for RC structures when applied to PT bridges shall be considered. No indications are provided about the number and the location of tests: suggestions can be found in CS 465:2020 [11] and FHWA (2013) [12] but the foreign guidelines must

* Corresponding author.
E-mail address: isabella.mazzatura@phd.unipi.it (I. Mazzatura).

https://doi.org/10.1016/j.istruc.2023.105314
Received 12 May 2023; Received in revised form 23 August 2023; Accepted 25 September 2023
Available online 10 October 2023

be adapted to the peculiarities of the Italian infrastructural heritage and the territory.

Given the relevance of the issue and the increasing scientific and technical interest, the need for well-defined procedures for assessing PT elements, including cables' location, defects' detection and quantification, and definition of the residual pre-stressing force in the structural components, become evident. The present work proposes an integrated methodology for the execution of in-situ inspections on PT bridges, providing reliable indications about techniques to be used, how to perform tests and the level of accuracy that shall be achieved. In some cases, testing techniques already used in different research fields are proposed, specifying the procedures to be adopted when applied to PT bridges, their pros and limitations: the application to in-situ viaducts can result in extreme difficulty due to the inherent complexity of the infrastructure, its dimensions, the interferences with normal activities, traffic loads, etc. Adjustments to procedures shall be therefore established, as well as acceptable errors in sight of their impact on the structural assessment.

The main novelty of the present research consists in trying to establish an integrated methodology for the inspection of post-tensioned bridges with bounded cables, knowing the relevance and the potential impact that hidden defects may have on their structural performance. Starting from a revision of the non-destructive techniques nowadays available and applying some of them, selected in relation to the deficiency to detect, both in controlled-laboratory conditions and in-situ, specific testing procedures are suggested.

The research represents the starting point for defining a more articulate and complete assessment procedure for PT bridges, which will involve detailed results about the reliability of the employed non-destructive techniques and indications about how to employ the outputs of the inspection in the accurate assessment.

2. The proposed inspection methodology

The proposed procedure aims at codifying the execution of in-situ inspections, thus evaluating the maintenance conditions of prestressed concrete bridges with PT cables, by focusing on three fundamental aspects (cables' tracing, localization and quantification of defects, determination of residual prestress force). The procedure is summarized as follows:

(a) *Visual inspections.* A first visual evaluation is needed to determine the overall condition of the bridge and the presence of visible defects affecting the concrete, the reinforcements, and the PT system (e.g. longitudinal cracks, moisture spots on cables, etc.).
(b) *Determination of the number of samples to investigate.* Lacking specific indications [10], the methodology proposed by the FHWA, adapted to the national infrastructural heritage and territory [13] can be used for this aim. The theoretical assumption consists in modelling the survey outputs (presence/lack of defects) through a hypergeometric distribution. The number of samples to test is then fixed by establishing the previously defined defectiveness level, assuming a percentage of elements showing defects and setting a confidence level.
(c) *Determination of the cables' layout.* The operation is necessary to organize and perform the in-situ investigations. In the presence of original drawings, their reliability regarding the state-of-design will be assessed.
(d) *Localization and quantification of voids/defects.* As degradation phenomena in PT beams are usually associated with inefficient grouting, suggested tests aim to locate voids within the ducts and assess the oxidation/corrosion occurrence in unprotected regions.
(e) *Determination of the actual prestressing force on post-tensioned components*. Since the residual tension acting on PT tendons influences the infrastructure's performance and depends on the cables' conservation conditions (point d), specific investigations are suggested.

Point *a)* is well discussed in the previously cited Guidelines, and in the Italian one especially. The determination of the number of samples deserves a specific and in-depth discussion, as is given in [13]. Here is possible to give only a brief and non-exhaustive discussion. The number of samples can be determined by following the approach suggested by the aforementioned American Standard [12]. In this context, the number of samples is obtained based on the assumption that the injection defects detected within the ducts can be described through a hypergeometric distribution. Assuming a certain percentage of defective cables, having set a target probability level, and knowing the total number of cables belonging to the considered population, it is possible to determine the sample size to investigate. The percentage of defective cables is assumed based on considerations regarding the risk associated with the structure and the impact of the chosen investigation techniques.

The present paper focuses on points (c), (d), and (e) of the proposed methodology. Different Non-Destructive Techniques (NDT) were selected, applied, compared, and calibrated through both tailored experimental laboratory tests and in-situ applications, providing reliable indications about how and where to perform tests for achieving a satisfactory knowledge level. Among all the possible methodologies provided by the current scientific literature, the choice of selected NDTs was based on the easiness and quickness of the in-situ application, the repeatability of the procedure, the specimens' preparation, etc. in sight of their adoption on a wide set of existing bridges owing different geometry, structural scheme, location, details, and environmental conditions. The adopted NDTs are briefly described with specific reference to the application field.

2.1. Determination of the cables' layout

The determination of the cables' layout along the structural component is necessary for the in-situ investigations. Knowledge about the path, the number, the typology of the cables, and the ducts' material is required. The use of low-impact techniques is strongly encouraged due to practical and safety reasons, but issues still exist about the most efficient methodology to adopt: the presence of a thick concrete cover, the surrounding reinforcements, and the ducts' material can negatively affect the tests' results.

Ground Penetration Radar (GPR) is considered the reference technique for tracing cables [14–19]. It is a radar imaging technique using electromagnetic pulses transmitted to the element at very high frequencies: the echoed signals are elaborated individuating the reflections generated by the metallic elements included in the concrete. GPR was widely used [20] for achieving information about reinforcements' layout [21–26], the position of prestressing strands and metallic ducts [20,22,26,27], and the presence of voids in the concrete.

The GPR operating mode consists of the tracing, on the selected element, of vertical lines with a pitch lower than 100 cm in the investigation area (Fig. 1). On each vertical line, a GPR scan is performed fixing directly on the element surface the position of the surveyed cable (Fig. 1, step 1); then, by connecting the so-obtained locations, it's possible to visualize the cables' traces (Fig. 1, step 2). Note that it is not often possible to investigate all the cables, for instance, the lower cable of the beam shown in Fig. 1 can't be located by the NDTs employed in the present research because of the high concrete cover and of the investigation surface slope. The beams to be investigated are selected in relation to their position and accessibility within the infrastructure.

2.2. Defects' localization

For PT beams, defects' detection corresponds to determining the presence of voids and water within the grouting: investigations shall focus on those areas with a higher probability of finding defects, i.e.

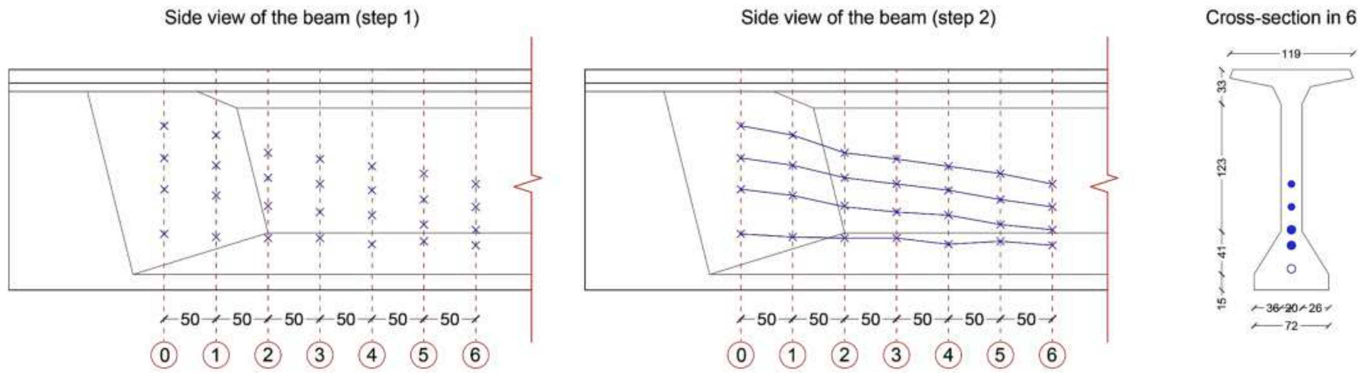

Fig. 1. Operative modality for GPR technique for cables' tracing: a) preparation of the surface of the beam and b) tracing operation in situ.

critical regions because of the geometry, presence of humidity spots, cracks, etc. To optimize resources, in terms of both time and economy, it is advisable to investigate all those areas for which the injection procedure was presumably more difficult [28], highlighted by way of example in Fig. 2, and the areas in which "warning" defects are present, that could be a symptom of a more serious defectiveness on the post-tensioned cable.

Many technologies exist to detect defects inside the ducts, e.g. thermography [29], X-ray [30] and gamma-ray imaging [31,32], Impact Echo (IE) [33–36], acoustic emission-based methods (i.e. Ultrasonic Echo (UE) and Ultrasonic Tomography (UT) [20,37–39]). To optimize results and minimize errors, more NDTs can be used [20].

UT was selected as the reference technique for the present application because of its quick and easy in-situ application; X-ray imaging was also used to verify the information given by UT, despite the high execution time and economic effort.

Historically, UT is a widely used technique for the evaluation of masonry structures, both for the identification of voids and for the detection of defects [40,41]. UT is reliable in estimating the thickness of elements/layers and in locating voids in PT ducts, especially when coupled with other testing methodologies [35,42]. A stress pulse is generated on the element's surface through a mechanical impact of one or more sensors, even working as receivers: part of the pulse propagates through the body, part is reflected and changes in the acoustic impedance are then captured. Through time-of-flight measurements, it is possible to locate discontinuities and therefore reinforcements, tendons, voids (cracks, honeycomb, delamination), or water defects [35]. UT works employing waves in the range frequency of 20–80 kHz.

From an operational point of view, drawing vertical lines 10 cm apart on the cables' trace is recommended. The choice of pitch extension depends on the smaller length of defects we want to detect with a pitch of 10 cm, defects longer than 10 cm will be well located. The instrument calibration is required, by imposing a sampling frequency in the range of 50 ÷ 60 kHz and an attempt velocity of around 2400 m/s if shear waves are used, as in the present research. Being the density (ρ) around 2500 $\frac{kg}{m^3}$, the Elastic modulus (E) equal to 34625 MPa (considering high-strength concrete) and the Poisson ratio (ν) equal to 0.18, the velocity of shear waves (c_t) can be estimated through Equation (1) [43]:

$$c_t = \sqrt{\frac{E}{\rho} \bullet \frac{1}{2 \bullet (1+\nu)}} = 2422\frac{m}{s} \tag{1}$$

where E is expressed in N/m^2 and ρ in kg/m^3.

After a few scans performed in the area with no ducts, it is necessary to check if the distance computed as $c_t \bullet t$ (being t the time required by the wave to come back) is comparable with the thickness of the investigated body. If strong differences are revealed, the assumed velocity needs to be changed. Besides, the analog and the digital gain shall be chosen, keeping attention to not overestimate the first one since unchangeable in the post-elaboration phase. By scanning two or more cables in sections where it is less likely to find voids, the analog and digital gain can be calibrated not saturating the displayed image. All sections with a high difference between the acoustic impedance of the preponderant material and that of the body encountered (i.e. with amplification) shall be marked.

Being UT a non-destructive technique, it is desirable to compare the results obtained with other technologies. To this aim X-ray imaging can be used, since able to provide two-dimensional images of the investigated area. Electromagnetic pulses are emitted by a tungsten X-ray tube and a photographic panel works as a receiver: the X-rays, passing through the object, are mitigated due to the higher density of eventual areas inside the object. A negative image in which the darker spots represent low-density areas, and the lighter spots represent high-density areas is then achieved.

2.3. Defects' entity quantification

The first step in quantifying the extent of defects is to perform endoscopic investigations where it had not been possible, through UT or any other NDT, to achieve reliable information, or where the localization phase had warned about potential defects. The execution of endoscopies requires the exact location of the cable. Since there is the practical risk of mashing the metallic duct on the cable making it difficult to analyze the resulting information (Fig. 3a), it is a good practice to first execute a hole of a bigger diameter (20 mm) and proceed then with a smaller diameter hole (10 mm) (Fig. 3b). In case of an evident lack of grouting, or oxidation/corrosion of the cable, it is recommended to

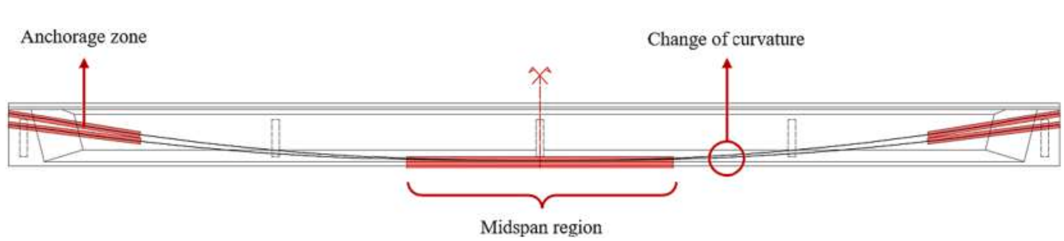

Fig. 2. Areas to investigate, from [13].

a) b) c)

Fig. 3. A) Poorly executed endoscopy: the mashed duct does not allow a correct evaluation; b) well-executed endoscopy: there is no grouting inside the duct; c) exposed cable with evident corrosion phenomena.

proceed with the removal of the concrete cover (Fig. 3c).

2.4. Definition of the actual tension

To estimate the efficiency of the PT system, it is possible to measure the tension acting through the steel cable by using the X-ray diffraction technique [44–46], widely adopted in the quality control industry to assess the residual stresses in steel components [47]. The X-ray diffraction method requires the cable to be exposed: the concrete cover, the metallic duct and the grouting shall be removed, as well as a certain amount of concrete nearby; the deeper the cable, the longer and wider the area to remove, to allow the motion of the diffractometer. The instrument shall be anchored to the beam, to avoid slip [45].

3. Laboratory and in-situ case studies

An extensive experimental campaign was performed, both in controlled-laboratory conditions and in-situ. Laboratory tests represent the preliminary step to calibrate reliable procedures for achieving the information required by the structural assessment. The so-calibrated procedures were applied in-situ on five different viaducts located on Northern Italy highways, allowing to assess the reliability of the approaches.

3.1. Laboratory specimens: Design and preparation

Laboratory tests were executed at the *Laboratorio Ufficiale per le Esperienze sui Materiali da Costruzione* of Pisa University (Italy). Four RC wall specimens, with strands located in ducts with different characteristics, were realized. Differences concerned *(a)* the ducts' material (metallic and plastic), *(b)* the ducts' location, and *(c)* the defect's size and typology. The variability of these parameters well represented what can be found in existing PT bridges.

Each specimen was characterized by the presence of six ducts: only metallic ducts in specimens n°1 and n°2, and both metallic and plastic ducts in specimens n°3 and n°4. The ducts were located respectively at 15 and 25 cm of depth from the left and right external sides. Specimens n°1 and n°2 presented, in five ducts, three defects (A, B, C) of increasing extension (3.0, 5.0, and 8.0 cm) and a fully grouted duct for comparison reasons. The eventual breaking of the duct, the strands, voids in the grouting, and the possible presence of water in the duct were also considered. To introduce defects into the specimens, different

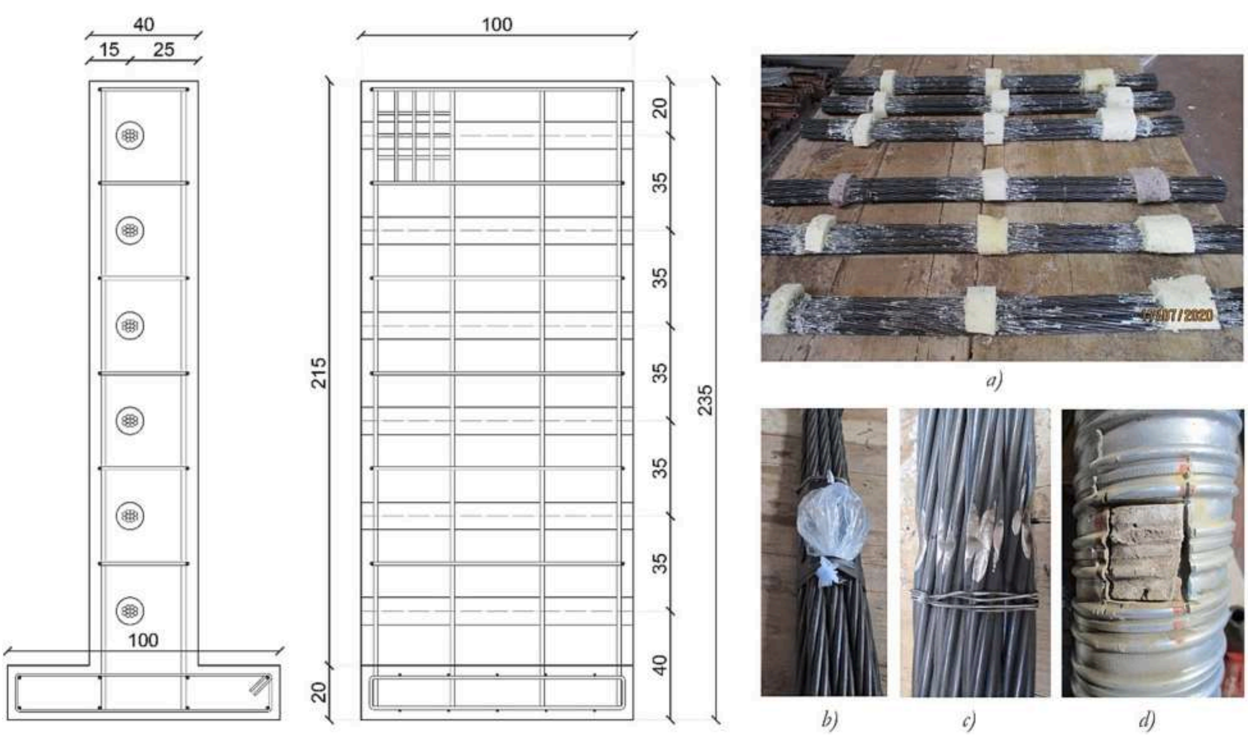

Fig. 4. On the left is the main geometrical dimension of the specimens; on the right are the techniques employed for the defects execution: a) void, b) water, c) break of the strands, d) break of the duct.

techniques were used, e.g. polyurethane foam to simulate the lack of grouting (Fig. 4a), plastic bags filled with water (Fig. 4b), and mechanical instrumentation to crack or break the strands or the metallic ducts (Fig. 4c–d). Table 1 summarizes information about the defects' location, extension, and typology.

3.2. In-situ case studies viaducts

Five viaducts, located on the highway system of Northern Italy and whose main features are given in Table 2, were selected for in-situ investigations. All the viaducts are composed of simply supported girder decks; the older viaducts have similar decks with double-T shape beams, while Bridge n.3 shows a T-beam transversal section. Information about the cables' layout (parabolic, as expected because of the simply supported static scheme), geometrical features, and mechanical properties was derived from the original documents.

4. Detection of strands in PT systems

4.1. Laboratory tests using GPR

Two different GPRs were used, provided by the *IDS Georadar Industry,* and owing different emission frequencies, equal to 2.0 and 3.0 GHz. The 2.0 GHz GPR (*C-thrue* model) consists of a box containing both the sensors and the results display screen, being a very handy, fast, and easy-to-use tool for a single operator. In particular, the instrument incorporates two antennas perpendicular-oriented to each other and spaced 10 cm. The dual polarization of the system allows for multi-level detection. In detail, the longitudinal polarization antenna can detect deeper objects than the transverse polarized one (the two channels are respectively represented in Fig. 5a) [15].

Table 1
Ducts and defects' typology.

Spec.	*Ducts and Defects' typology*			
	ID	***duct***	***Grouting***	***defect and location***
1	M1	metallic	complete	
	M2	metallic	partial (right side)	semi-circular voids of 3, 5, and 8 cm extension.
	M3	metallic	partial (left side)	semi-circular voids of 3, 5, and 8 cm extension.
	M4	metallic	partial (left side)	water defects of 3, 5, and 8 cm extension.
	M5	metallic	partial (right side)	voids in a sector-circular shape of 3, 5, and 8 cm extension.
	M6	metallic	partial (left side)	voids in a sector-circular shape of 3, 5, and 8 cm extension.
2	M7	metallic	complete	broken duct
	M8	metallic	complete	cuts on strands of increasing penetration (minor in A, major in C).
	M9	metallic	partial (lower side)	voids of 3, 5, and 8 cm extension.
	M10	metallic	partial (lower side)	water defects of 3, 5, and 8 cm extension.
	M11	metallic	partial (upper side)	voids in a sector-circular shape of 3, 5, and 8 cm extension.
	M12	metallic	partial (right side)	water defects of 3, 5, and 8 cm extension.
3	P13	plastic	complete	void in the centre (8 cm extent).
	P14	plastic	complete	void in the centre (22 cm extent).
	P15	plastic	complete	void in the centre (33 cm extent).
	P16	plastic	complete	
	M17	metallic	complete	void in the centre (33 cm extent).
	M18	metallic	complete	void in the centre (22 cm extent).
4	P19	plastic	complete	water in the centre (20 cm extent).
	P20	plastic	partial (half grouted, half empty)	
	P21	plastic	total empty	
	P22	plastic	total grouted	
	M23	metallic	partial (half grouted, half empty)	
	M24	metallic	complete	water in the centre (20 cm extent).

The 3.0 GHz GPR has two separate bodies, i.e. the sensor (TR-SHF antenna model) and the screen, then requiring the contemporaneous presence of (at least) two operators and resulting in less practical and fast respect to the other one (Fig. 6). The instrument was used to assess the presence of strands and defects in the laboratory RC wall specimens, resulting very efficient in locating the strands except in those areas with the congested presence of rebars. Fig. 6 shows, for instance, the results provided by the 2.0 GHz GPR applied to specimen n.1: the ducts are visible along the whole specimen's length, except at the top, presenting a large amount of longitudinal and transversal reinforcement (Fig. 4). No differences are observed in the scan if there was a defect.

4.2. In-situ tests using GPR

The two systems adopted for lab investigations were used to analyze 24 beams located in the different in-situ viaducts (3 on Bridge n.1 and Bridge n.3, 7 on Bridge n.2, 4 on Bridge n.4, and 7 on Bridge n.5) and to identify the cables' layout. GPR tests were performed on the vertical face of the beam, approximately in the first 7 ÷ 8 m from the heads. In the case of double T-shaped beams, due to a thick concrete cover and geometrical discontinuities, it was not possible to perform tests in the bulb area along the whole longitudinal extension; also, the beam's intrados surface in the mid-span region was difficult to analyze due to reinforcement and cables' congestion, disturbing the signal. Tests were then concentrated in the areas close to the head of the beam from the vertical web face. The attempt investigation pitch was equal to 50 cm, a good compromise considering the time and amount of collected data. Every 50 cm, a vertical scan was made over the height of the beam, identifying the cables' position. Fig. 7 shows the GPR test execution in situ.

For all the analyzed viaducts, the in-situ measurements highlighted very low deltas from the design cables' trace, with maximum differences in the order of 10 cm. Fig. 8 shows some examples of the comparison between the cables' layout coming from in-situ measures (continuous lines in blue and cyan) and design drawings (red dotted lines).

The tests were performed following the procedure previously explained by different inspectors but ever supervised by the same researcher, to minimize the operators' errors. Besides, endoscopic investigations were performed on the viaducts to confirm the effective position of the cables: the 56 endoscopies performed on Bridge n.5 and the 3 on Bridge n. 2 revealed the cable in the exact location provided by the GPR.

For the error evaluation, the following methodology was adopted: GPR measurements were first compared to the design previsions, by assuming the execution coincided with the state of design (i.e. design VS in-situ). The difference between the design value and the average of the GPR measures was calculated for each cable and each section. The GPR data were then compared to each other to assess the in-situ variability of the cable trace (i.e. in-situ VS in-situ), by assuming, in turn, one of the inspected beams as a reference and by performing the same calculations. Absolute values were considered to make the results comparable in the two considered situations. Fig. 9 contains the boxplots of the two considered scenarios, and Table 3 summarizes the values of interest (median, the maximum errors, and the interquartile range (IQR) of the absolute values). The median error is comparable in the two scenarios, except for bridges n.3 and n.5, perhaps suggesting a variation between the execution and the design of the cable' trace. The IQR gives information about the dispersion of the data, and it is always higher in the second scenario. This can be due to the slight and inevitable variations in the positioning of the ducts during manufacturing operations. Fig. 10 shows the histograms of the errors. Data are presented discretizing, on the x-axis, errors in ranges of 3.0 cm, being the diameter of the bridge ducts equal to 6.0 cm and the GPR locating the axis of the duct. Errors within 3.0 cm (i.e. the first interval of the histogram) are then acceptable.

Table 2
Main characteristics of the viaducts (L total length, L_s single span length, ft ultimate tensile strength).

Bridge	Year	N_{spans}	L (m)	L_s (m)	N_{beams} /span	N_{cables} /beam	Cables' typology	f_t (MPa)	Initial pre-stress
1	1964–1965	18 (11PT, 7 RC)	500	30–24	3	4–5	Parallel wires	Unknown	Known
2	1973–1974	8	290	32–37	4	5	Strands	1′800	Unknown
3	1989	11	420	30–38	6	4	Unknown	Unknown	Unknown
4	1972	14	570	39–41	3	7	Parallel wires	1′480	Known
5	1976	14	600	34–40-45	4	4-5-6	Parallel wires	1′600	Unknown

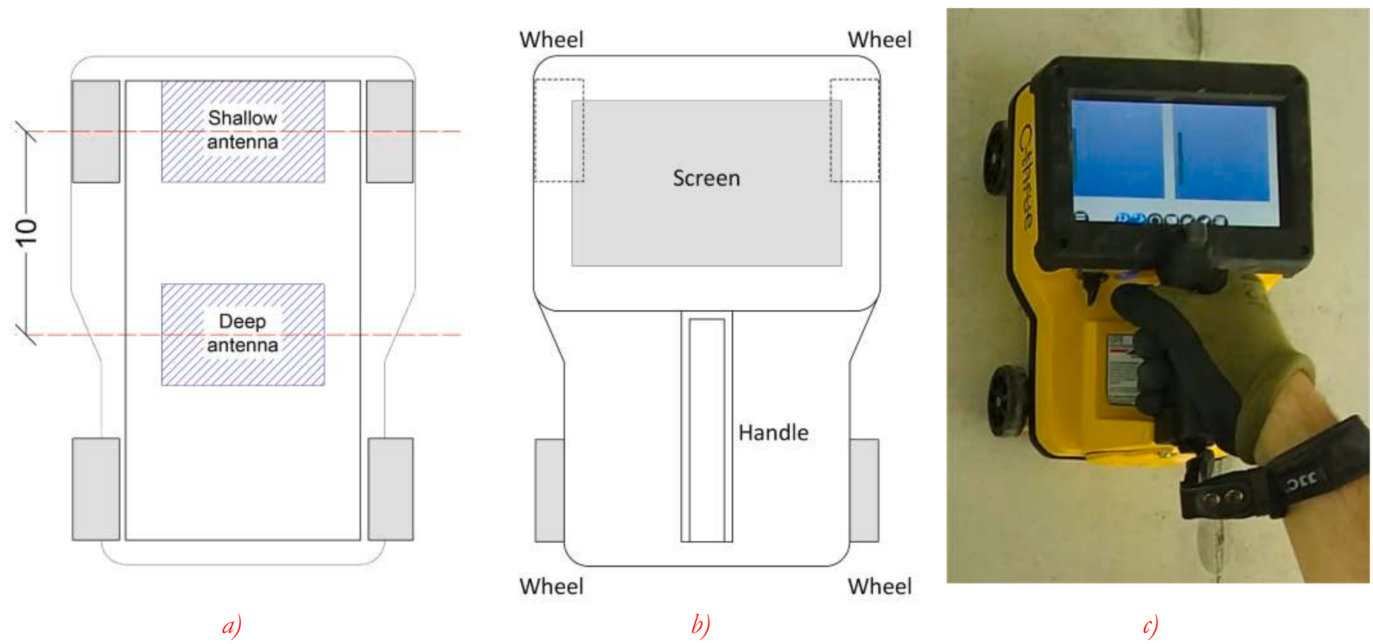

Fig. 5. A) Plan upside-down view of the GPR with location of the two antennas; b) plan view of the GPR; c) actual view of the GPR.

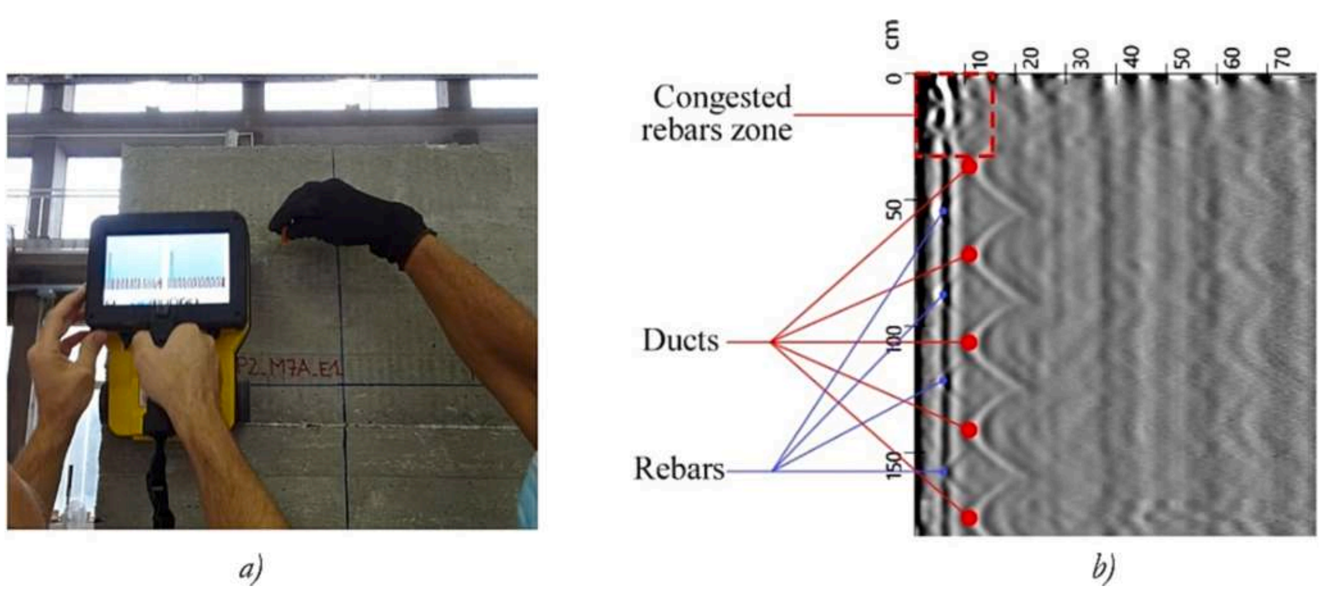

Fig. 6. A) GPR 2 GHz tests on specimens in Pisa Lab with; b) GPR 2 GHz radargram result of the cross-section of the specimen n.1.

5. Detection and quantification of voids and defects

5.1. Laboratory tests using ultrasonic tomography

Two different devices were used for UT tests, both using an array of Dry Point Contact (DPC) transducers emitting shear waves and not requiring a preliminary preparation of the concrete surface or the employ of a coupling gel. The first device (A1040 MIRA) consists of 12 blocks of 4 transducers: each block works as a single emitting/receiving sensor; Fig. 11 shows a schematic representation of the instrument: in a)

Fig. 7. GPR execution in situ.

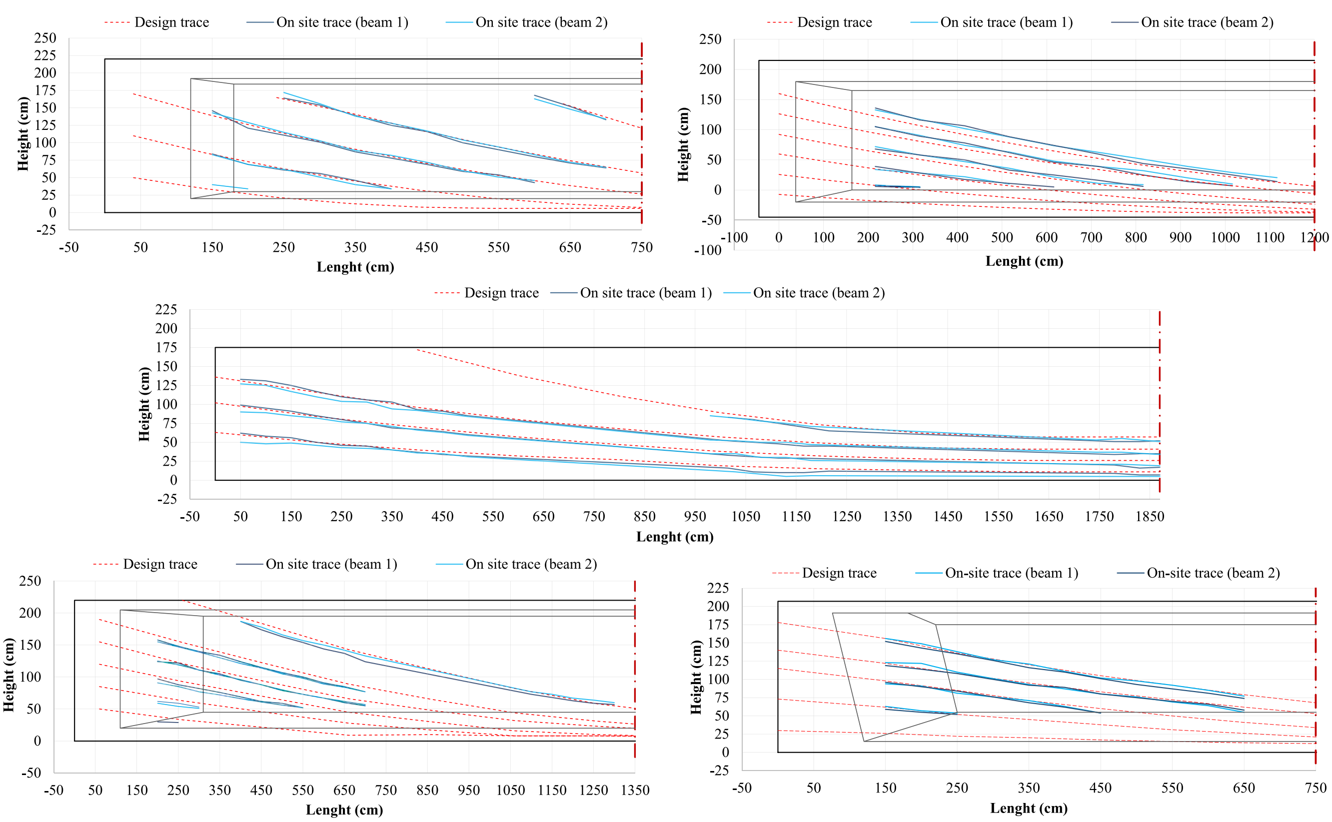

Fig. 8. Comparison of cables trace according to in-situ measurements (blue) and design state (red) for two beams of the different case studies: a) Bridge n.1, b) Bridge n.2, c) Bridge n.3, d) Bridge n.4 and e) Bridge n.5. (For interpretation of the references to colour in this figure legend, the reader is referred to the web version of this article.)

the plan view is given, while in b) the side one. Fig. 11b) shows also the linear mode working: the linear array 1 is the emitter while the other arrays are the receiver; then, in turn, each linear array is set as the emitter and the others as receivers. In approximately 3 s, a set of 66 waveforms can be collected in the time domain (A-Scan) and computed as tomographic scans (B-scan, C-scan) using the Synthetic Aperture Focusing Technique (SAFT) [48,49]. The device is provided by a screen, allowing the visualization of the B-scan result. The second device (A1040 MIRA 3D) is more compact, lighter, and easier to handle. The functioning and the device itself are roughly the same as the MIRA 1040, rather than the number of the emitting/receiving transducers (32, 8 blocks of 4 transducers) and the possibility of achieving “Matrix scans”, i.e. the function whereby each transducer can work alone [50] and the possibility of visualize C-scans and D-scans during the tests’ execution.

The experimental laboratory campaign consisted of the execution of several series of scans performed by placing the device transversely to the duct. The number of scans depends on the chosen pitch (here 10 cm), influencing the acquisition time required and the minimum size of the defect to be recognized (the smaller the pitch, the smaller the size of the defect that could eventually be found).

Investigations focused on the best choice for the analog gain and the digital gain by fixing the emission frequency at 55 kHz (i.e. best compromise considering the concrete [43]) and by knowing the wall thickness (and therefore setting emission velocity). Such parameters need to be deeply investigated since strongly influence the results of the test: the SAFT algorithm provides a colour map representing the acoustic impedance variation between the base material and the object material in the section scanned: a poor choice of the analog gain may be

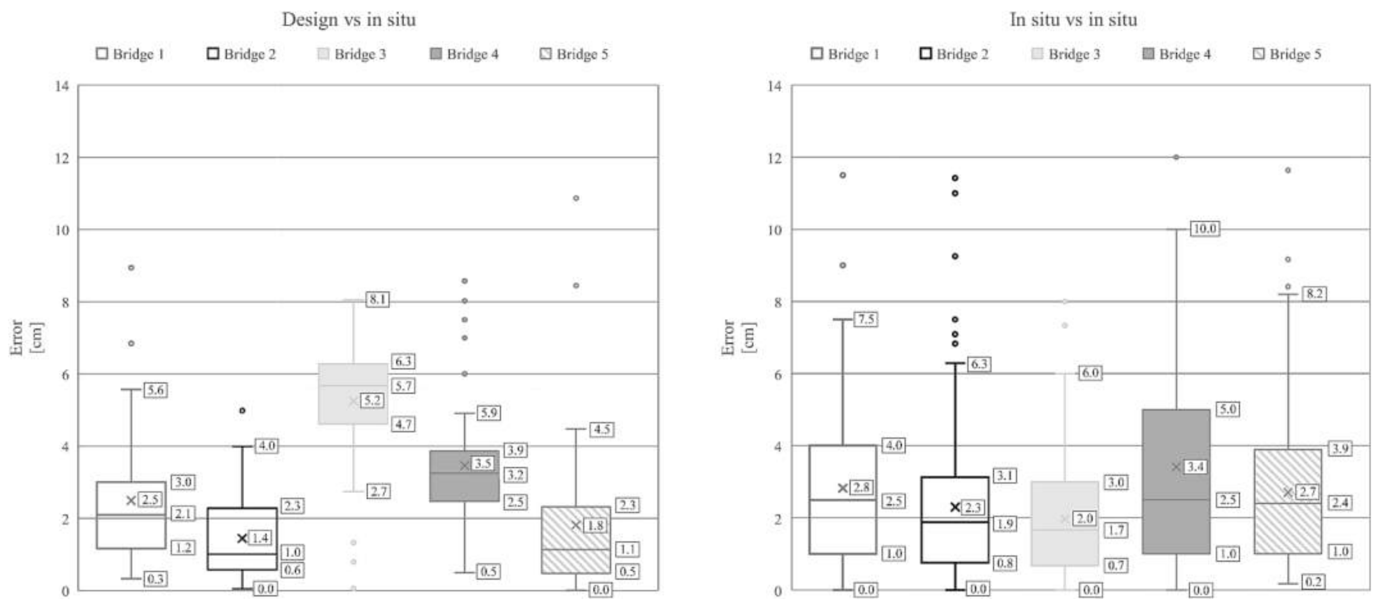

Fig. 9. Boxplots of the absolute errors in the two considered scenarios (Design vs in situ and in situ vs in situ). The points are the outliers. The mean, the median, the first and the second interquartile, and the minimum and the maximum error are represented.

Table 3
GPR method, values of interest.

Bridge ID	Design vs in-situ					In-situ vs in-situ				
	Median error [cm]	Max. error [cm]	IQR [cm]	N° Outliers	Tot. sample	Median error [cm]	Max. error [cm]	IQR [cm]	N° Outliers	Tot. sample
n.1	2.1	5.6	1.8	2	31	2.5	7.5	2.9	2	90
n.2	1.0	4.0	1.6	1	43	1.9	6.3	2.3	6	203
n.3	5.7	8.1	1.6	3	47	1.7	6.0	2.3	2	183
n.4	3.2	4.9	1.3	5	46	2.5	10.0	4.0	1	62
n.5	1.1	4.5	1.7	2	34	2.4	8.2	2.9	3	203

responsible for a high delta and a low delta to appear as the same in the scan, making useless the result of the investigation.

UT allows determining the presence of air or water inside the metallic duct, without distinguishing water from the air. Fig. 12 shows the results of the UT application to RC specimens. Fig. 12a (duct M2, specimen 1) highlights the presence of defects A and C (in red) of an extension within 3 and 8 cm; defect B is, otherwise, not visible as a consequence of employing a 10 cm pitch dimension. With more extended defects, (e.g. Fig. 12b–e) the scans are more reliable, even if the deepness of the investigation highly affects the result: the higher the concrete cover, the worst the scan's result (Fig. 12e). Fig. 12c shows a fully grouted plastic duct, which UT scan is completely saturated: the shear waves velocity through a plastic material is almost null, as in the case of water and air. Fig. 12d evidences the consequences of congestion of steel reinforcements, making it impossible to distinguish the duct, similar to GPR tests. The results of the scans are summarised in Fig. 13. A total of 190 scans were performed, running in both linear and matrix modes, and slightly changing the analog gain value. Results are organized by assigning a 'hit' when the defect is detected and a 'miss' when it is not. The larger the defect size, the higher the 'hit' rate; however, it would be advisable to extend the sample by simulating more defects of different lengths to provide a more reliable assessment of the NDT.

5.2. In-situ tests using Ultrasonic Tomography and X-ray imaging

In addition to UT, X-ray scans were also adopted to detect defects on in-situ viaducts. The surveys focused on the cables, analyzing, in particular, those areas with a higher probability of finding defects because of operational difficulties during grouting execution, i.e. near the anchor, in the change of curvature areas, or in the mid-span region where the cables are horizontal. Surveys were similarly organized for all the inspected viaducts, being almost the same as the static scheme and the strands' pattern. 20 beams were investigated using UT (3 beams on Bridge n.1, 6 on Bridge n.2, 2 on Bridge n.3, and Bridge n.4 and 7 on Bridge n.5), while the X-rays scan method was applied on 4 beams (2 on Bridge n.2 and 2 on Bridge n.4).

Ultrasonic Tomography. The calibration operations were performed as for the lab tests, fixing the velocity of the emission wave by knowing the thickness of the inspected area. It was necessary to first trace the cables using GPR (because the tomographic scans were made transversely to the duct) and then to divide the drawn trace into a constant pitch of 10 cm. Fig. 14 shows the execution of the UTs in situ.

The main issues were related to the superficial finishing of the concrete: in the presence of considerable roughness, because of honeycombs and/or poor repairs, the scans were inconsistent (Fig. 15a). The scans made from the intrados in the midspan region of the beams were also very disturbed because of the strong amount of steel (reinforcements and ducts). In Bridge n.2 and n.4 tomographic scans from the intrados were performed: it was neither possible to distinguish the ducts (Fig. 15b). High values of digital gain may significantly affect the imaging of the scans (Fig. 15c), making it impossible to provide exact values to be used for the investigation since depending on several highly variable parameters (e.g. the concrete quality). Then, values of digital gain that led to a very saturated image should be considered as not

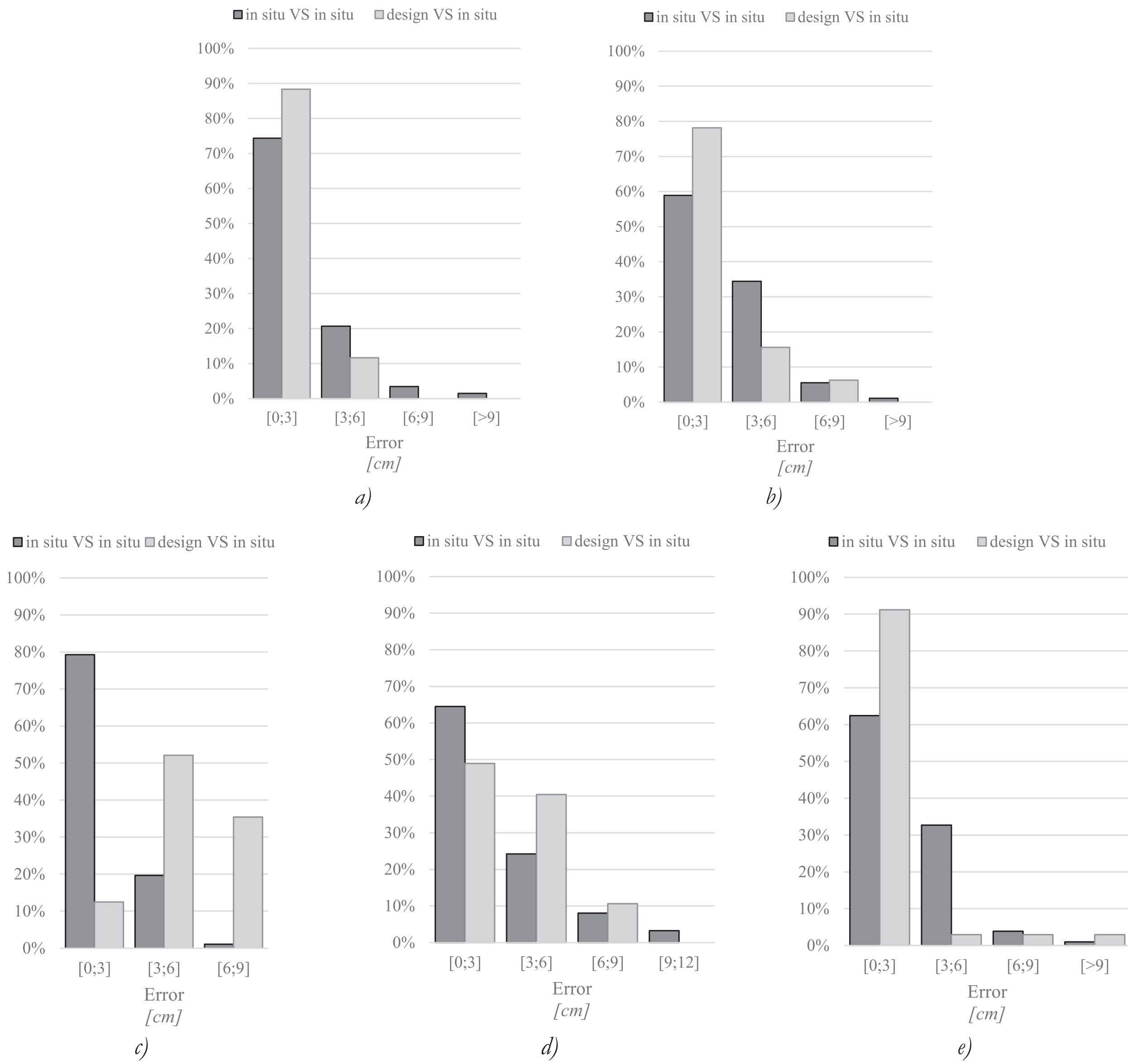

Fig. 10. Histograms of the absolute error for a) Bridge n.1, b) Bridge n.2, c) Bridge n.3, d) Bridge n.4, and e) Bridge n.5.

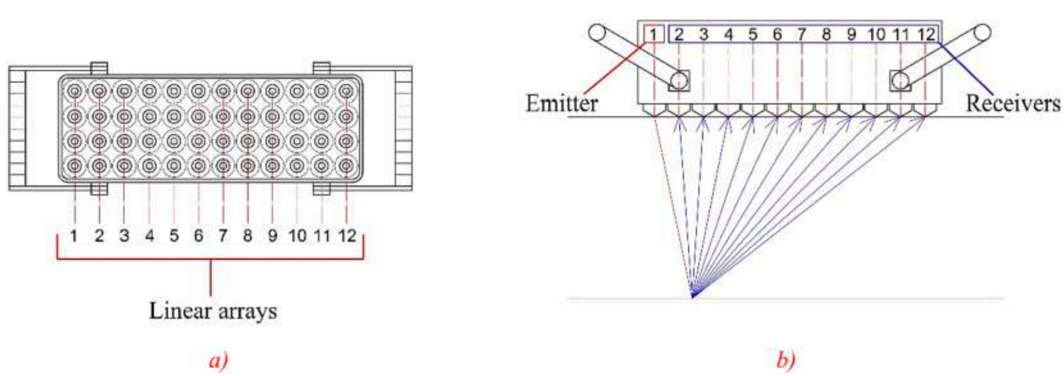

Fig. 11. A) Plan view of the tomograph; b) side view of the tomograph showing the working modality: the linear array 1 is the emitter, while the others are the receivers.

reliable.

For Bridge n.2 matrix scans were also performed. Due to time effort in executing the matrix modality, the decision was to investigate a large part of the viaduct using the linear modality and proceed with the matrix mode only in the potentially defective areas (Fig. 16). In the case of badly executed repairs, the linear and the matrix scans are both not

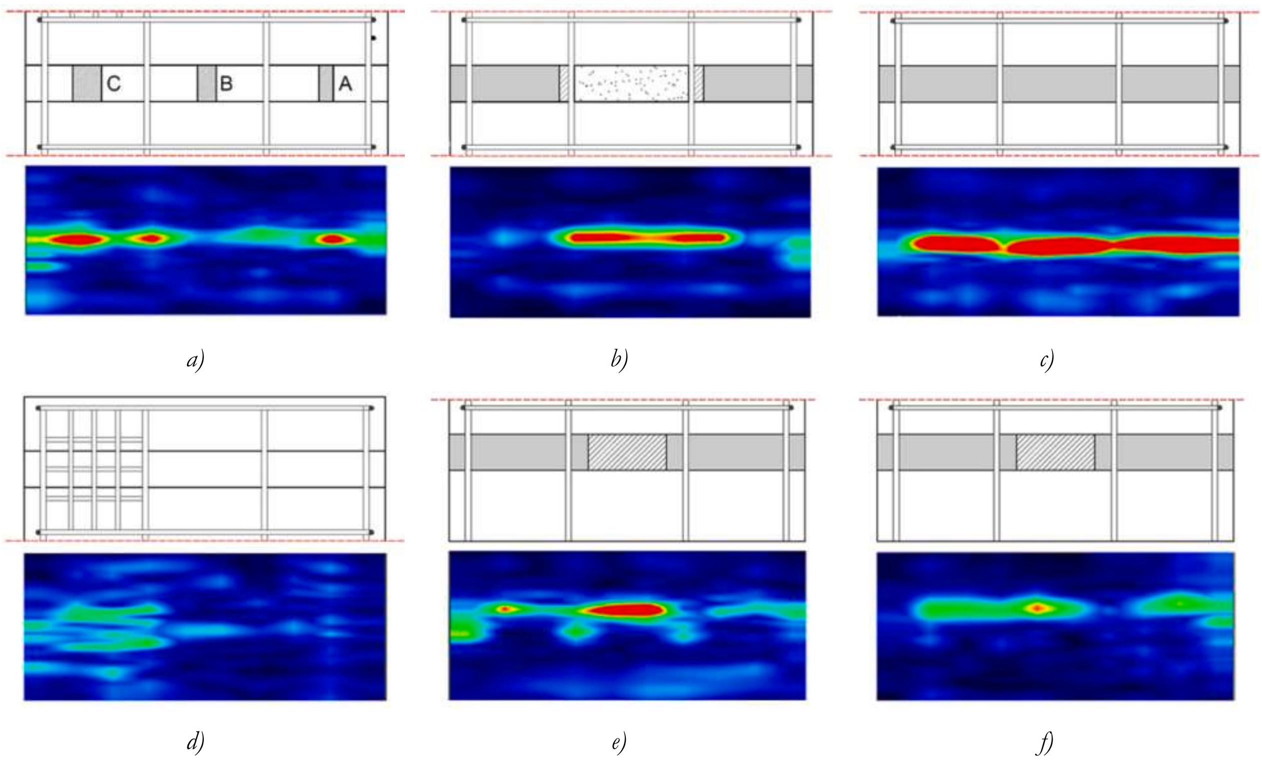

Fig. 12. Efficacy of UT scans: a) void defects from 3 (A) to 8 cm (C); b) defect of 40 cm c) Plastic duct with NO voids, d) Influence of a concentrated presence of steel; e) defect of 22 cm, the duct is 15 cm depth; f) same defect of e) but the duct is 25 cm depth.

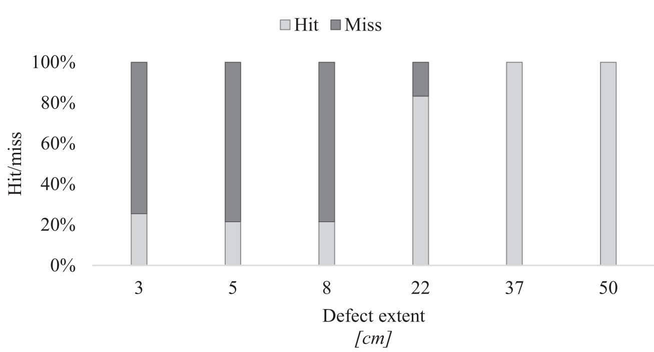

Fig. 13. Hit and miss rates.

relevant. If the linear scan is amplificated, the corresponding matrix scan is not enforced amplificated too. Where both the scan modalities give amplification, the presence of defects is highly probable.

On Bridge n.2, endoscopic investigations were also performed and used for assessing the effective presence of voids warned through the application of UT by investigating both amplified areas (54% of the total) and not amplified or not detectable areas by UT (intrados region, rough concrete surface). Endoscopic investigations performed in warned UT areas confirmed voids in 63% of cases but in 4 cases the void was outside the ducts. The random tests reported the presence of defects in 23% of the cases.

The main issue in the UT application is, therefore, the eventual presence of voids in correspondence with the ducts, (e.g. when being detached from the concrete matrix), because it is not possible to distinguish this kind of void from the one located inside the ducts. Then, it is suggested to perform the UTs together with some endoscopies.

X-rays scan. X-ray scans were applied on Bridge n.2 and Bridge n.4. Radiographic technologies require many precautions since radiation are involved. More in details, Fig. 17 and Fig. 18 show respectively the side view and the cross-section of the inspection site. A radiation-protected van shall be located close to the inspection truck, where the operators, expert radiologists, can monitor the progress of the work. The apparatus to perform the radiographic scan is composed of an emitter and a photographic panel working as a receiver (Fig. 18 and Fig. 19). A single scan has a size of 20 cm × 20 cm and requires from 5 to 15 sec to be performed, in relation to the width to be inspected. Considering the time required for placing the transmitters (in the present campaign moved manually) and the operators' movement (to the inspection truck and then to the van for starting the acquisition), the actual time to perform one single scan is around 15 min, being therefore the procedure quite time-demanding.

The radiographic scan methodology provided good results in terms of localization of the steel elements (both cables and ordinary bars), while, for what concerns the detection of voids, the procedure was efficient only if the defects were not located behind steel elements. High-density materials, like steel, tend to absorb a large part of the radiation not allowing us to see what is behind or in front of it. Fig. 20 shows the results of the X-ray scan application to Bridge n.4: in general, voids are visible, in Fig. 20a a honeycomb inside the section can be noticed, while in Fig. 20b a continuous void longitudinal to the duct was observed. However, the rebars and wires absorb a large part of the radiation, therefore in correspondence of its nothing else can be detected. Moreover, in one of the viaducts, the radiographic scans were made on a beam with several broken wires in a strand. Still, the radiographic scan did not allow us to appreciate the defect. In conclusion, the radiographic technique results very expensively in terms of time and money, requires many cautions in-situ, and gives not reasonably clear information about the state of conservation.

6. Quantification of actual prestressing force

6.1. Laboratory tests using X-rays diffraction method

The X-ray diffraction technique investigates the near-surface sample

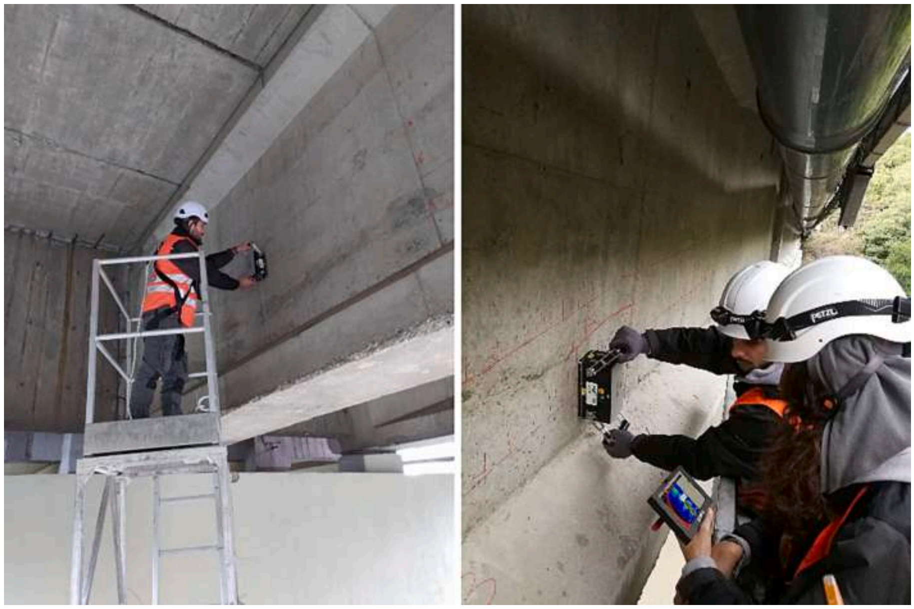

Fig. 14. UT execution in situ.

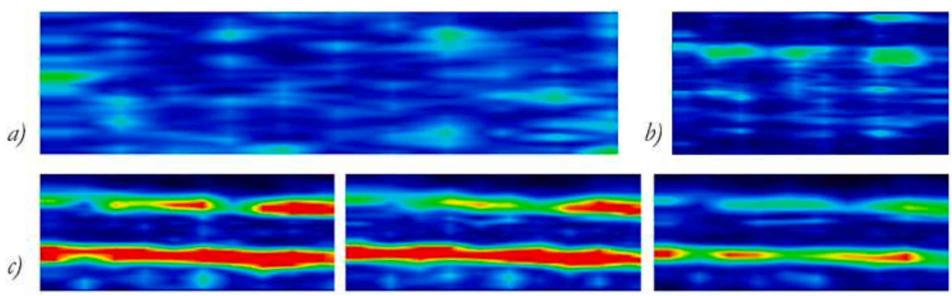

Fig. 15. A) scan made from rough surfaces (presence of honeycombs) on a beam belonging to the bridge n.1; b) scan made from the intrados of a beam of bridge n.2c) Three scans of the same area with decreasing digital gain (Bridge n.3, beam 1, span 4).

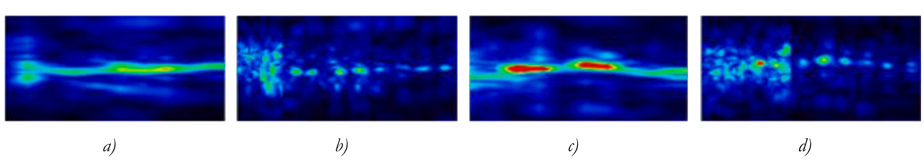

Fig. 16. a) and c) are linear tomographic scans, and b) and c) are the corresponding matrix, both affected by roughness. The scans were made on beam 4, span 2 of the Bridge n.2.

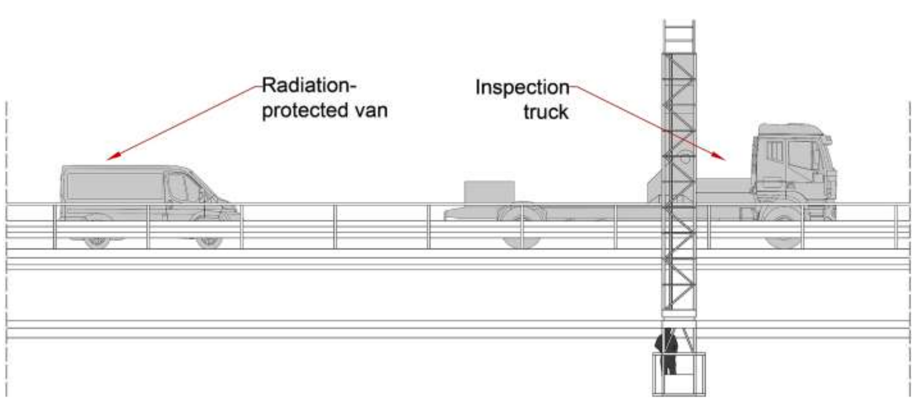

Fig. 17. Side view of the in-situ operation to perform X-ray scans.

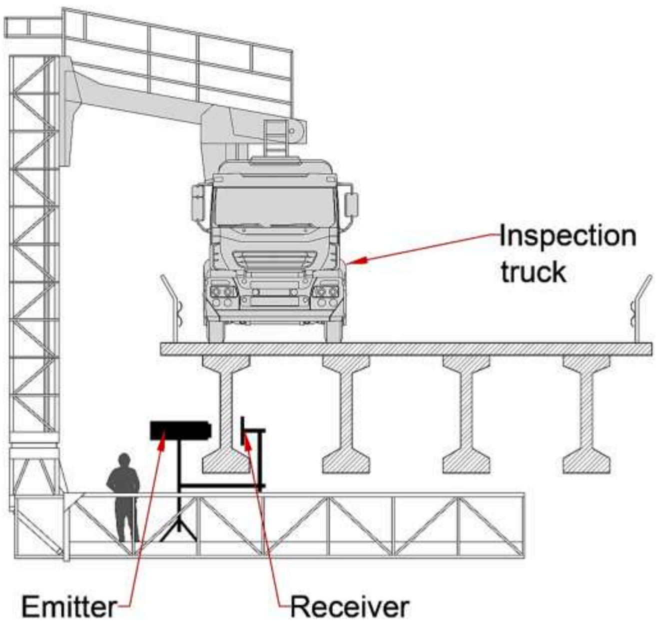

Fig. 18. Cross section of the in-situ operation to perform X-rays scans.

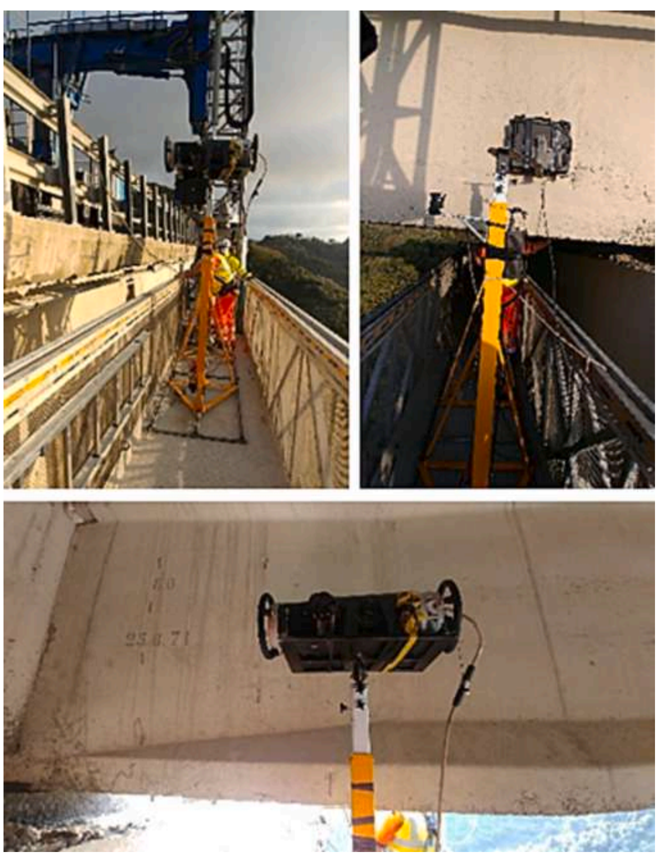

Fig. 19. Some views of the emitter and the receiving panel.

region (about 10 μm), estimating the stress as a function of the interplanar spacing between the crystalline lattice planes, assuming linear elastic distortions. Several methods exist to estimate the residual stresses in metallic materials, such as the single-angle, the two-angle, $\sin^2\psi$, etc.) [51]. In the present campaign, the $\sin^2(\psi)$ method was used to evaluate the acting stress. Equation (2) can be adopted for the stress measurement:

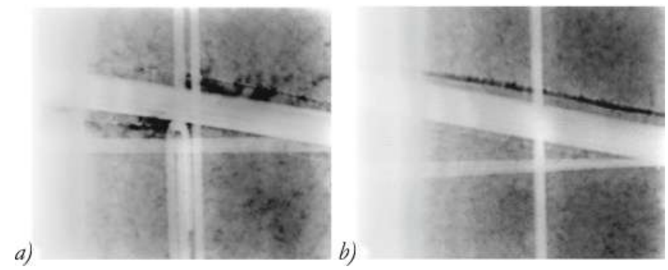

Fig. 20. A) Honeycombs inside the concrete (bridge n.4); b) voids in the upper part of the duct (bridge n.4). Note that behind the vertical bar, it is not possible to see the void.

$$\frac{d_{\phi\psi} - d_0}{d_0} = \left(\frac{1+\nu}{E}\right)\sigma_\phi sin^2(\psi) - \left(\frac{\nu}{E}\right)(\sigma_1 + \sigma_2) \tag{2}$$

being E the Young's modulus, ν the Poisson's ratio normal to the *(hkl)* orientation of the material (i.e. the values for the crystallographic direction normal to the lattice planes in which the strain is measures as specified by the Miller indices *(hkl)* [51]), d_0 the interplanar distance at stress-free condition (inherent property of each crystalline material [52]) and σ_ϕ the interplane stress with respect to the two principal stress components σ_1 and σ_2. Under certain assumptions, Equation (2) can be rewritten as (3):

$$\sigma_\phi = \left(\frac{E}{1+\nu}\right)_{hkl}\frac{1}{d_0}\left(\frac{\delta d_{\psi\phi}}{\delta \sin^2\psi}\right) \tag{3}$$

The main assumption of the method is that plain stress is applied. By the Bragg law, it is possible to estimate $d_{\phi\psi}$, i.e. the interplanar distance in the stress condition. Then, these strain values can be determined by measuring the $\sin^2\psi$ values at different orientations, i.e. varying ψ. The strain values are therefore used to calculate the stress by fitting the experimental data to the $\sin^2\psi$ equation [53].

In the present campaign, for a single determination of a $d_{\phi\psi}$ lattice spacing, i.e. a single stress measure, 9 measures were performed by varying ψ angle (in the range of $\pm 35°$), with a counting time of 45 s; the stress was defined by a least square minimization of the regression equation. A portable Spider TM X GNR diffractometer was employed, working at 30 kV and 90 μA with a radiation source of chromium.

The experimental laboratory campaign, described and discussed in [45], was executed to prove the efficiency of the X-ray diffraction method in quantifying the prestressing force on PT tendons and assessing the repeatability of the measurements. Four samples were chosen, different for typology (single wire, wire strand) and diameter (Table 4).

The test was carried out by tensioning the samples at various load levels and measuring the acting tension. Two different test setups were adopted. The single wire and the 7-wire strand of diameter 9.30 mm were tested through a standard Instron® machine with a total capacity of 200 kN. The other samples were tested through a relaxation testing machine [54,55] since a uniform stress distribution through the strands

Table 4
Geometrical dimensions of the studied wire and strands and the number of tests.

Element	d_{int} [mm]	d_{ext} [mm]	L_{win} [mm]	Effective area [mm^2]	N° of tests
5.20 Single wire	5.20		–	21.24	17
9.30 7-wire strand	3.30	3.10	140	53.84	9
15.20 7-wire strand	5.20	5.00	140	139.05	24
15.70 7-wire strand	5.40	5.20	210	150.34	13

was more easily obtained.

A critical analysis of the data is given in [45]; to summarize, it can be stated that even if the experimental campaign is limited, a good correlation was identified between the effective tension (known since imposed and since every specimen was instrumented through a strain gauge rosetta) and the measured one through the X-ray technique: for the typical working load (60% of yielding stresses) the methodology can assess the acting force in a range of about ± 10%, while for lower working loads the range increases up to ± 30%.

6.2. In-situ tests on prestressing steel

The X-ray diffraction technique was applied on 2 of the bridges for determining the pretension force on steel strands. From a practical point of view, the most relevant issue concerns the positioning of the instrument, needing to be anchored to the beam and requiring a long preparation time and extreme caution. The execution of a direct essay to uncover the cables and to allow the instrument's motion is necessary. Once the duct is open, the mortar grouting was manually removed with a chisel. In the presence of oxidation phenomena, the application of a pickling agent is necessary. Before restoring the concrete cover after measurements, cables shall be protected by applying a passivating treatment.

Measurements were executed in the middle span intrados of the beam, repeating the measure, for each cable, at least three times. The repetition of each measure is performed to validate the results obtained since the in-situ measurements could be affected by a major uncertainty because of the possible occurrence of unexpected situations (i.e. movements/vibrations because of the traffic). Table 5 summarizes results in terms of mean stress values, CoV (estimated on each cable), hypothetical actual tension, and the maximum percentage difference between the latter value and the mean of the in-situ ones. The actual tension was estimated based on the cables' trace, the mechanical properties of materials, and the whole span geometry – available through both original drawings and results of in-situ tests. However, lacking information about the design's tension of the cables in the viaducts, a prestressing tension equal to 70% of the ultimate tensile strength of the steel ($f_{u,k}$) was assumed, in agreement with national standards in force at realization time [56]. The friction losses and the time-dependent losses were calculated, the latter according to the Eurocode 2 [57] formulations.

For Bridge n.2 viaduct, a residual acting tension of 990 MPa was estimated, being $f_{u,k}$ 1800 MPa and having 23% of total losses; for Bridge n.5, a residual acting tension of 855 MPa was achieved considering $f_{u,k}$ equal to 1570 MPa and the total losses up to 22%.

As visible from Table 5, the measured stresses measured were lower than the estimated ones and this could be due to the presence of compressive residual stresses deriving from manufacturing processes [46]. The first cracking moment was computed to assess the reliability of the X-ray measurements. For both structures, it resulted that the beams would show cracks if the level of prestressing force in the cables was the measured one. The limit tension value for the beam not to be cracked would be 760 MPa in the Bridge n.2 case and 670 MPa in the n.5: underestimations of at least 120 MPa and 35 MPa exist respectively for Bridge n.2 and n.5 by considering the average value of the measures. The Bridge n.2 cables are composed of strands, therefore the higher Δ between the measured value and the minimum one for the beam not to be cracked could be due to the non-uniform distribution of the stresses in the strands cross section, as reported in [58]. Indeed, by considering the coefficient proposed by Morelli et al. [45], the difference between the measured value and the minimum value for the beam not to be cracked goes to 70 MPa.

Anyway, the achieved data can be considered satisfactory overall: the maximum coefficient of variation (CoV) calculated on the measurements performed on each beam amounts to 8%, by considering the measures normally distributed. However, since there are no differences in structural terms for the beams belonging to the same viaduct, the value of acting stress should be more or less the same for all beams. For Bridge n.2, maximum variations of 148 MPa are observed, and for Bridge n.5 of 100 MPa. A reason for this range and also for the Δ with the expected value, as hypothesized in [46], could be the difference in compressive residual stresses induced by the operation of drawing the cables through the ducts.

7. Conclusions and future developments

Prestressed concrete bridges with post-tensioned cables represent a large percentage of the Italian infrastructure stock, progressively approaching the end of their useful life. Given the inherent nature of this type of structure, the execution of in-situ inspections is very complex. The potential presence of hidden defects, not detectable by visual inspections further complicates the matter.

The present research work aims to define an integrated inspection methodology for PT bridges. The identification of the fundamental characteristics to be investigated is the preliminary step of the inspection process: the definition of the cable layout, the location, and quantification of hidden defects, and the determination of the level of actual tension in the PT system are all aspects to be accurately considered. Executing investigations on such structures requires costly operations (traffic total/partial closures, use of inspection platforms, careful design of the safety plan), which must be properly considered. The selection of investigation technologies was executed based on *(i)* time-consuming/costly execution and *(ii)* the effectiveness of the investigation technique.

The first point was decisive in the selection of the technologies to be applied, while the second was only partially addressed, mostly providing a statistical analysis of the data collected. Therefore, the research is still in progress, lacking the reliability quantification of the selected investigation techniques.

To select and calibrate the methodologies to be adopted for each of the above-mentioned aims, a preliminary laboratory test campaign in well-controlled conditions was performed, allowing the validation of the procedure to be further applied to existing viaducts opportunely selected as case studies. The chosen methodologies are well known in the scientific community, and the present research aimed to test their effectiveness and applicability in-situ to codify a clear inspection procedure

Table 5
X-ray diffraction method, values of interest.

Structure	PT system	Span	Beam	Number of tests	Mean measured tension [MPa]	Standard deviation [MPa]	CoV	Analytical tension [MPa]	Δ% between measurements and analytical values
Bridge n.2	Strands	2	4	12	692.33	40.35	6%	990	30%
		3	4	3	601.67	46.32	8%		39%
		3	3	6	708.33	39.34	6%		28%
		6	3	3	568.33	30.35	5%		43%
		6	4	6	560.17	37.89	7%		43%
		7	4	3	699.67	28.18	4%		29%
Bridge n.5	Wires	3	1	4	648.00	47.81	7%	855	24%
		3	3	8	685.88	41.21	6%		20%
		6	2	5	569.20	36.00	6%		33%

that is as objective as possible.

GPR was assessed as a valid and easy technique for detecting the cables' layout by comparing it to information derived from original documentation. Ultrasonic Tomography was defined as a reliable testing procedure to locate defects along the cables and the ducts and to quantify their entity, but it is suggested to perform it together with other testing methodologies, because of the possible occurrence of false positives outputs (i.e. when the voids are external to the duct). The X-ray diffraction method was validated to be effective in the evaluation of the residual prestressing force on cables, with the general tendency of an underestimation. The application of the proposed integrated approach was validated with some positive results when applied to existing viaducts located along the Italian highway. Further in-situ applications are planned to refine the procedure, and further laboratory tests are provided to quantify the reliability of each of the survey techniques considered since the actual sample is not significant for this aim.

Declaration of Competing Interest

The authors declare the following financial interests/personal relationships which may be considered as potential competing interests: Walter Salvatore, University of Pisa (Principal Investigator for the Research) reports financial support was provided by SINA S.p.A.

Acknowledgments

The authors would like to acknowledge SINA Site Service S.p.A. (ASTM Group) for the possibility to execute the tests in-situ and for supporting the research; In particular, Eng. Filippo Ferrari and Eng. Andrea Piscini for their help during in-situ operations. Thanks to the colleagues from the University of Padua for the X-ray diffraction measurements on one of the structures, Prof. Manuele Dabalà, Luca Pezzato, and Claudio Gennari. All the laboratories that participated in the tests' execution are thankfully acknowledged (Boviar, IDS GeoRadar, In-situ, Tecno Piemonte 2Effe Engineering, and 2F Lab).

References

[1] Vereecken E, Botte W, Lombaert G, Caspeele R. Assessment of corroded prestressed and posttensioned concrete structures: A review. Struct Concr 2021;22:2556–80. https://doi.org/10.1002/suco.202100050.
[2] Anania L, Badalà A, D'Agata G. Damage and collapse mode of existing post tensioned precast concrete bridge: The case of Petrulla viaduct. Eng Struct 2018; 162:226–44. https://doi.org/10.1016/j.engstruct.2018.02.039.
[3] Li F, Yuan Y, Li CQ. Corrosion propagation of prestressing steel strands in concrete subject to chloride attack. Constr Build Mater 2011;25:3878–85. https://doi.org/10.1016/j.conbuildmat.2011.04.011.
[4] Dai L, Wang L, Zhang J, Zhang X. A global model for corrosion-induced cracking in prestressed concrete structures. Eng Fail Anal 2015;62:263–75. https://doi.org/10.1016/j.engfailanal.2016.01.013.
[5] Podolny W. Corrosion of Prestressing Steels and Its Mitigation. PCI J 1992;37: 34–55. https://doi.org/10.15554/pcij.09011992.34.55.
[6] Hong S, Wiggenhauser H, Helmerich R, Dong B, Dong P, Xing F. Long-term monitoring of reinforcement corrosion in concrete using ground penetrating radar. Corros Sci 2017;114:123–32. https://doi.org/10.1016/j.corsci.2016.11.003.
[7] Wang L, Zhang X, Zhang J, Ma Y, Xiang Y, Liu Y. Effect of insufficient grouting and strand corrosion on flexural behavior of PC beams. Constr Build Mater 2014;53: 213–24. https://doi.org/10.1016/j.conbuildmat.2013.11.069.
[8] Carsana M, Bertolini L. Corrosion failure of post-tensioning tendons in alkaline and chloride-free segregated grout: a case study. Struct Infrastruct Eng 2015;11: 402–11. https://doi.org/10.1080/15732479.2014.887736.
[9] Menga A, Kanstad T, Cantero D, Bathen L, Hornbostel K, Klausen A. Corrosion-induced damages and failures of posttensioned bridges: A literature review. Struct Concr 2023;24(1):84–99.
[10] MIT CSLP. Linee Guida per la classificazione e gestione del rischio, la valutazione della sicurezza ed il monitoraggio dei ponti esistenti. 2020.
[11] Highways England. CS 465 - Management of post-tensioned concrete bridges 2020.
[12] FHWA. Guidelines for Sampling, Assessing, and Restoring Defective Grout in Prestressed Concrete Bridge Post-Tensioning Ducts 2013.
[13] Mazzatura I, Caprili S, Salvatore W, Lupoi A. A multi-phase survey approach for post-tensioned prestressed concrete bridge decks 2023. https://doi.org/10.1201/9781003323020-487.
[14] Wai-Lok Lai W, Dérobert X, Annan P. A review of Ground Penetrating Radar application in civil engineering: A 30-year journey from Locating and Testing to Imaging and Diagnosis. NDT E Int 2018;96:58–78. https://doi.org/10.1016/j.ndteint.2017.04.002.
[15] Pasculli D, Natali A, Salvatore W, Morelli F, Morandi D. Investigation of reinforced concrete bridges by using a dual-polarized high-frequency GPR. In: 2018 17th International Conference on Ground Penetrating Radar, GPR 2018. Institute of Electrical and Electronics Engineers Inc.; 2018. https://doi.org/10.1109/ICGPR.2018.8441633.
[16] Liu S, Weng C, Jiao P, Wang F, Fu L, Meng Xu, et al. GPR signal analysis of post-tensioned prestressed concrete girder defects. J Geophys Eng 2013;10(3):034005.
[17] Giannopoulos A, Macintyre P, Rodgers S, Forde MC. GPR detection of voids in Post-Tensioned concrete bridge beams. 2002.
[18] Sławski Ł, Kosno Ł, Świt G. Evaluation of Precast Pre-post-tensioned Concrete Bridge Beams with the Use of GPR Method. Procedia Eng 2016;156:443–50.
[19] Pollock DG, Dupuis KJ, Lacour B, Olsen KR. Detection of Voids in Prestressed Concrete Bridges using Thermal Imaging and Ground-Penetrating Radar. 2008.
[20] Terzioglu T, Karthik MM, Hurlebaus S, Hueste MBD, Maack S, Woestmann J, et al. Nondestructive evaluation of grout defects in internal tendons of post-tensioned girders. NDT E Int 2018;99:23–35.
[21] Beben D, Mordak A, Anigacz W. Identification of viaduct beam parameters using the Ground Penetrating Radar (GPR) technique. NDT E Int 2012;49:18–26. https://doi.org/10.1016/j.ndteint.2012.03.001.
[22] dos Santos VRN, Al-Nuaimy W, Porsani JL, Hirata NST, Alzubi HS. Spectral analysis of ground penetrating radar signals in concrete, metallic and plastic targets. J Appl Geophy 2014;100:32–43. https://doi.org/10.1016/j.jappgeo.2013.10.002.
[23] Soldovieri F, Persico R, Utsi E, Utsi V. The application of inverse scattering techniques with ground penetrating radar to the problem of rebar location in concrete. NDT E Int 2006;39:602–7. https://doi.org/10.1016/j.ndteint.2005.12.005.
[24] Shaw MR, Millard SG, Molyneaux TCK, Taylor MJ, Bungey JH. Location of steel reinforcement in concrete using ground penetrating radar and neural networks. NDT E Int 2005;38:203–12. https://doi.org/10.1016/j.ndteint.2004.06.011.
[25] Pasculli D, Natali A, Salvatore W, Morelli F, Morandi D. Investigation of reinforced concrete bridges by using a dual-polarized high-frequency GPR. In: 2018 17th International Conference on Ground Penetrating Radar, GPR 2018 2018:1–5. https://doi.org/10.1109/ICGPR.2018.8441633.
[26] Kohl C, Streicher D. Results of reconstructed and fused NDT-data measured in the laboratory and on-site at bridges. Cem Concr Compos 2006;28:402–13. https://doi.org/10.1016/j.cemconcomp.2006.02.005.
[27] Clem DJ, Schumacher T, Deshon JP. A consistent approach for processing and interpretation of data from concrete bridge members collected with a hand-held GPR device. Constr Build Mater 2015;86:140–8. https://doi.org/10.1016/j.conbuildmat.2015.03.105.
[28] Trejo D, Pillai R, Beth M, Hueste D, Gardoni P. Parameters influencing corrosion and tension capacity of post-tensioning strands. ACI Mater J 2009;106:144–53.
[29] Garrido I, Lagüela S, Otero R, Arias P. Thermographic methodologies used in infrastructure inspection: A review—post-processing procedures. Appl Energy 2020;266:114857. https://doi.org/10.1016/j.apenergy.2020.114857.
[30] Innocenzi RD, Pigliapoco G, Carbonari S, Gara F, Dezi L. Damage Detection of Post-tensioned Cables in Existing Bridges with Digital Radiography. Lecture Notes in Civil Engineering. In: 200 LNCE. Springer Science and Business Media Deutschland GmbH; 2022. p. 662–9. https://doi.org/10.1007/978-3-030-91877-4_75.
[31] Mariscotti BMAJ, Jalinoos F, Frigerio T, Ruffolo M, Thieberger P. Gamma-Ray Imaging for Void and Corrosion Assessment Safety and utility of the technology make it appropriate for field application 2009.
[32] Freij H, Dukeman D, Alexander CL, Ruffolo MD, Frigerio T, Boselli J, et al. Comparison of novel imaging sensor and gamma ray tomography imaging of grout deficiencies in external post-tensioned structural tendons. NDT E Int 2021;117: 102368.
[33] Carino NJ. The impact-echo method: An overview. In: Structures - A Structural Engineering Odyssey, Structures 2001 - Proceedings of the 2001 Structures Congress and Exposition, vol. 109, 2004. https://doi.org/10.1061/40558(2001)15.
[34] Carino NJ, Sansalone M. Detection of voids in grouted ducts using the impact-echo method. Mater J 1992;89:269–303.
[35] Muldoon R, Chalker A, Forde MC, Ohtsu M, Kunisue F. Identifying voids in plastic ducts in post-tensioning prestressed concrete members by resonant frequency of impact-echo, SIBIE and tomography. Constr Build Mater 2007;21:527–37. https://doi.org/10.1016/j.conbuildmat.2006.04.009.
[36] Tinkey Y, Olson LD. Applications and limitations of impact echo scanning for void detection in posttensioned bridge ducts. Transp Res Rec 2008;2070(1):8–12.
[37] Schickert M. Ultrasonic NDE of concrete. Proc IEEE Ultrason Symp 2002;1:739–48. https://doi.org/10.1109/ultsym.2002.1193506.
[38] Schickert M, Krause M, Mü LW. Ultrasonic Imaging of Concrete Elements Using Reconstruction by Synthetic Aperture Focusing Technique. J Mater Civ Eng 2003; 15. https://doi.org/10.1061/ASCE0899-1561200315:3235.
[39] Iyer SR, Sinha SK, Schokker AJ. Ultrasonic C-scan imaging of post-tensioned concrete bridge structures for detection of corrosion and voids. Comput Aided Civ Inf Eng 2005;20(2):79–94.
[40] Valluzzi MR, Mazzon N, Munari M, Mazzon N, Munari M, Casarin F, et al. Effectiveness of injections evaluated by sonic tests on reduced scale multi-leaf masonry building subjected to seismic actions. NDTCE'09. Non-Destruct Test Civ Eng 2009.
[41] Schuller M, Berra M, Atkinson R, Binda L. Acoustic tomography for evaluation of unreinforced masonry. Constr Build Mater 1997;11(3):199–204.

[42] Martin J, Broughton KJ, Giannopolous A, Hardy A, Forde MC. Ultrasonic tomography of grouted duct post-tensioned reinforced concrete bridge beams. NDT&E Int 2001;34:107–13. https://doi.org/10.1016/S0963-8695(00)00035-9.
[43] Krautkrämer J, Krautkrämer H. Ultrasonic Testing of Materials. Springer Berlin Heidelberg; 1990. https://doi.org/10.1007/978-3-662-10680-8.
[44] Brauss ME, Pineault JA, Belassel M, Teodoropol SI. Nondestructive, quantitative stress characterization of wire rope and steel cables. 1998.
[45] Morelli F, Panzera I, Piscini A, Salvatore W, Chichi F, Marconi GP, et al. X-ray measure of tensile force in post-tensioned steel cables. Constr Build Mater 2021; 305:124743.
[46] Carfagno MG, Noorai FS, Brauss ME, Pineault JA. Extending the Lifespan of Structures. vol. 73. 1995.
[47] Lu J. Handbook of measurement of residual stresses. 1996.
[48] Elbern AW, Guimarães L V, Elbern AW. Synthetic Aperture Focusing Technique for Image Restoration B-scan Image Restoration Algorithm Based on Synthetic Aperture Focusing Technique (SAFT). 1999.
[49] Stepinski T, Lingvall F. Synthetic aperture focusing techniques for ultrasonic imaging of solid objects. In: 8th European Conference on Synthetic Aperture Radar, Aachen: 2010, p. 1–4.
[50] ACS Group. A1040 MIRA 3D Operation manual Ultrasonic low-frequency tomograph. 2021.
[51] Prevey PS. X-ray diffraction resiual stress techniques. ASM Handbook 1986;10: 380–92.
[52] British Standards Institution. Non-destructive Testing - Test Method for Residual Stress analysis by X-ray Diffraction. 2008.
[53] Luo Q, Jones AH. High-precision determination of residual stress of polycrystalline coatings using optimised XRD-sin2ψ technique. Surf Coat Technol 2010;205: 1403–8. https://doi.org/10.1016/j.surfcoat.2010.07.108.
[54] Gucci N. Un apparato per misure di rilassamento su acciai da precompresso. Atti Dell'Istituto Di Scienza Delle Costruzioni Dell'Università Di Pisa 1964;n. 111, V: 190–209.
[55] Gucci N. Un apparato di precisione per misurare il rilassamento dei trefoli da precompresso. Atti Dell'Istituto Di Scienza Delle Costruzioni Dell'Università Di Pisa 1968;n. 160, IX:241–57.
[56] Ministero dei Lavori Pubblici. Norme tecniche alle quali devono uniformarsi le costruzioni in conglomerato cementizio, normale e precompresso ed a struttura mettalica. 1972.
[57] Eurocode 2: Design of concrete structures - Part 1-1: General rules and rules for buildings. 2004.
[58] Ma J, Guo Y. Stress analysis of steel wire in strand based on optical lever principle and finite element calculation. J Braz Soc Mech Sci Eng 2020;42(1).